Polarization-dependent manipulation of optical properties in a tripod system

Santosh Kumar,[1] Thomas Lauprêtre,[2] Fabien Bretenaker,[2] Fabienne Goldfarb,[2] and Rupamanjari Ghosh[1,3,*]

[1]*School of Physical Sciences, Jawaharlal Nehru University, New Delhi 110067, India*
[2]*Laboratoire Aimé Cotton, CNRS, Université Paris-Sud 11, ENS Cachan, 91405 Orsay Cedex, France*
[3]*School of Natural Sciences, Shiv Nadar University, Gautam Budh Nagar, Uttar Pradesh 203207, India*

We analyze the dependence of the transmission profiles of an atom in a tripod configuration on the polarizations of the coupling and the probe beams and use room-temperature metastable helium (^{4}He*) as a model system. We show that, by rotating the orthogonally polarized coupling-probe beams with respect to an applied small magnetic field, one can manipulate the detuned peaks due to electromagnetically induced transparency [Kumar, Lauprêtre, Ghosh, Bretenaker, and Goldfarb, Phys. Rev. A **84**, 023811 (2011)] and the central peak arising because of ground-state coherent population oscillations [Lauprêtre, Kumar, Berger, Faoro, Ghosh, Bretenaker, and Goldfarb, Phys. Rev. A **85**, 051805(R) (2012)] observed earlier separately. Our experimental results match well with our numerical simulation using the Floquet method.

I. INTRODUCTION

The effect termed as electromagnetically induced transparency (EIT) is a well-known phenomenon of quantum interference in a three-level Λ system, which leads to the cancellation of absorption of a resonant probe in the presence of a coupling beam [1–3]. It is a two-photon process, and the width of the EIT resonance is limited by the Raman coherence lifetime involving the two lower levels of the Λ. EIT has many applications in a variety of research areas, such as slow and fast light [4–7], light storage [8], quantum memory [9–11], sensitive magnetometers [12,13], quantum nonlinear optics [7,14], quantum-information processing [10,15], and quantum networking [16].

Extensions of the usual three-level EIT to multilevel schemes have led to a number of interesting and potentially useful coherence effects, such as coherent superposition of quantum states using stimulated Raman adiabatic passage [17–19], interacting dark resonances [20,21], Zeeman coherent oscillations in degenerate duplicated two-level systems [22] and nondegenerate duplicated two-level systems [23], and magneto-optical rotation and cross phase modulation via coherently driven tripod systems [24]. We also have experimentally and theoretically demonstrated interacting EIT resonances in a tripod system of hot atomic vapor of metastable helium [25] subjected to a weak magnetic field, in which the three optical transitions in the tripod are excited separately by the probe and coupling beams, with either two probed transitions or two coupling transitions on the side legs.

A completely different effect that can give rise to very narrow transmission resonances occurs in two-level atomic systems and is called coherent population oscillations (CPO) [26,27], in which the beat note between a coupling beam and a coherent probe beam leads to a temporal modulation of the population difference between the excited and ground levels. The dispersion associated with CPO resonances has led to applications such as slow and fast light for microwave photonics [28–30]. As this phenomenon is limited by the

population decay rate of the upper level, it leads to resonances that are usually broader than EIT ones. Nevertheless, we have observed CPO phenomena in a three-level Λ system using room-temperature metastable ^{4}He (^{4}He*) with a linewidth even narrower than the one achieved by EIT in the same system [31]. This is due to a transfer of CPOs to the lower levels of the Λ system. Such a CPO transfer has already been seen in the case of absorption resonances by Berman *et al.* [32], and Goren *et al.* [33] predicted a few years ago that very narrow absorption resonances can more generally be achieved in cycling degenerate two-level transitions, where $F_e = F_g + 1$ and $F_g \geqslant 1$, interacting with pump and probe lasers of the same polarization. Recently, it has been theoretically suggested that CPO resonances can be applied in spatial optical memories [34] or narrowband biphoton generation [35].

Given the interest in such transparency resonances, the importance of a clear understanding of their diverse origins, proven by unambiguous experimental demonstrations, cannot be overemphasized. The system of room-temperature ^{4}He* offers itself as a model in which the different effects of EIT and CPO can be combined and probed effectively. As is already well known, ^{4}He* has some peculiar favorable properties.

(i) Velocity changing collisions enable us to span the entire Doppler profile [36].

(ii) The absence of nuclear spin simplifies the level scheme and eliminates the need for repumping lasers compensating for losses into the other ground-state hyperfine levels.

(iii) Diffusive motion increases the transit time of the atoms through the laser beam and hence the Raman coherence lifetime.

(iv) Collisions with the ground-state atoms do not depolarize the colliding ^{4}He*. Thus there are no background atoms to contribute to noise.

(v) Penning ionization among identically polarized ^{4}He* atoms is almost forbidden [37].

In this paper, we again consider a four-level tripod system of ^{4}He*. The excited state $2\,^3P_0$ ($m_e = 0$, $|e\rangle$) of ^{4}He* can be coupled selectively to the $2\,^3S_1$ sublevels, $m_g = -1$ ($|g_-\rangle$), 0 ($|g_0\rangle$), and $+1$ ($|g_+\rangle$), by copropagating laser beams at around 1083 nm, with σ^+, π, and σ^- polarizations, respectively. The energy separation between the $2\,^3P_0$ and

*rghosh.jnu@gmail.com

the next lower sublevel $2\,^3P_1$ is large (29.6 GHz) compared to the Doppler width ($\lesssim 1$ GHz), allowing one to ensure that each transition is isolated. This is not the case, for example, in Rb [33,38]. By rotating the polarization of mutually orthogonal coupling-probe beams, we create intermediate cases of the two basic tripod configurations explained in Ref. [25], now with possible mixing of the excitations on each of the three optical transitions in the tripod. In this four-level "double" tripod configuration, we record the transmission profiles in the presence of an applied magnetic field and for different combinations of orthogonal polarizations of coupling and probe beams on the three transitions. We observe detuned EIT peaks together with a central CPO resonance in the intermediate cases. EIT peaks shift with increasing magnetic field and for different combinations of coupling and probe polarizations and split into two or four peaks. The central narrow CPO resonance, limited only by the decay rate of ground-state populations, appears for some intermediate cases of the coupling and probe polarizations and disappears in the extreme cases of Ref. [25]. The strong dependencies of the transmission profiles on the external magnetic field, coupling Rabi frequency, and coupling-probe polarizations lend themselves to suitable control and manipulation.

The paper is organized as follows. In Sec. II, we describe the experimental setup. In Sec. III, we present the model of the four-level tripod system using the Floquet method. In Sec. IV, we present the experimental results and compare them with our numerical simulations based on the Floquet method. Our conclusions are presented in Sec. V.

II. EXPERIMENTAL SETUP

The experimental setup is similar to the one in Ref. [25] and shown in Fig. 1(a). The helium cell is 6 cm long, has a diameter of 2.5 cm, and is filled with ^{4}He at 1 Torr. The cell is placed in a three-layer μ-metal shield to isolate it from stray magnetic field inhomogeneities. Helium atoms are excited to the metastable state by a rf discharge at 27 MHz. We use
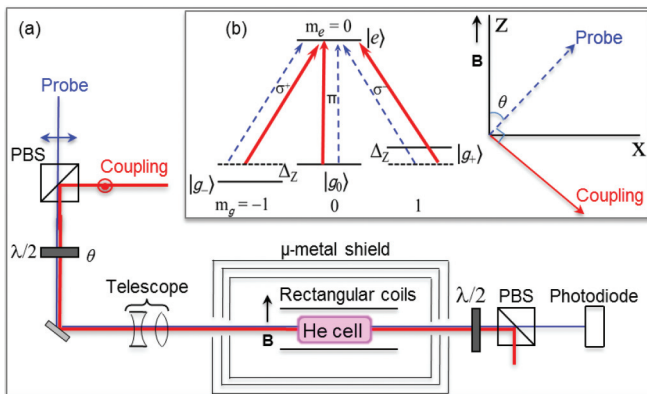

FIG. 1. (Color online) (a) Experimental setup. PBS: polarizing beam-splitter, $\lambda/2$: half-wave plate. (b) Four-level tripod system with perpendicularly polarized probe (blue dashed line) and coupling (red continuous line) beams. θ is the angle between the probe polarization and the Z axis. The Z axis is fixed by the direction of the magnetic field B so that $\theta = 0$ gives a π probe and a σ coupling. Δ_Z is the Zeeman splitting.

the $2\,^3S_1 \rightarrow 2\,^3P_0$ transition of ^{4}He* (D_0 line). The coupling and probe beams are derived from the same 1083-nm diode laser, and their frequencies and intensities are controlled by two acousto-optic modulators (not shown). The probe power of about 100 μW is small compared to the milliwatt range of the coupling power. A variable weak magnetic field (B) generated by a pair of rectangular coils surrounding the helium cell removes the degeneracy of the lower Zeeman sublevels. These coils produce a horizontal magnetic field perpendicular to the direction of propagation of the laser beams. A polarizing beam-splitter (PBS) is used to recombine the two beams, and a $\lambda/2$ wave plate changes the relative angle between the coupling and probe beams and the quantization axis defined by the magnetic field. The coupling and probe beam diameters are about 1 cm after the telescope as they enter the helium cell.

III. THEORETICAL FORMULATION AND STEADY-STATE SOLUTION BY FLOQUET METHOD

We consider a four-level tripod system, with perpendicularly polarized coupling and probe beams of Rabi frequencies Ω_C and Ω_P, respectively [Fig. 1(b)]. The direction of the magnetic field B is taken as the quantization axis Z. For the helium $2\,^3S_1$ state, the Landé g factor is 2.002. The magnetic field shifts the metastable $2\,^3S_1$ (m_J) state by $\mu_B B m_J g$, where $\mu_B = e\hbar/2m_e = 9.274 \times 10^{-24}$ J/T is the Bohr magneton. This gives the Zeeman splitting, $\Delta_Z \equiv \mu_B B m_J g/h = 2.8$ kHz for $B = 1$ mG. The Rabi frequency of the coupling beam Ω_C is much larger than the Zeeman splitting Δ_Z.

The Hamiltonian of the system can be expressed as

$$\mathbf{H} = \mathbf{H_0} + \mathbf{H_I}. \tag{1}$$

$\mathbf{H_0}$ is the unperturbed Hamiltonian,

$$\mathbf{H_0} = \sum_i \hbar\omega_i |i\rangle\langle i|, \tag{2}$$

where $i = e, g_-, g_0, g_+$ corresponds to the different levels, labeled in Fig. 1(b). $\mathbf{H_I}$ is the interaction Hamiltonian,

$$\mathbf{H_I} = -\frac{\hbar}{2} e^{-i\omega_C t}[X_2|e\rangle\langle g_0| + X_1(|e\rangle\langle g_-| + |e\rangle\langle g_+|) + \text{H.c.}], \tag{3}$$

where $X_1 = (\Omega_P e^{-i\delta t}\sin\theta + \Omega_C \cos\theta)/\sqrt{2}$, $X_2 = -(\Omega_P e^{-i\delta t}\cos\theta - \Omega_C \sin\theta)$, and δ is the frequency difference between the probe and the coupling beams. θ is the angle between the probe beam polarization and the magnetic field, as shown in Fig. 1(b). For $\theta = 0$, the probe is π polarized and the coupling is σ polarized, while it is the other way for $\theta = \pi/2$. In these two cases, the probe and coupling beams excite the three optical transitions separately, while an intermediate θ mixes the excitations on each transition.

The time evolution of the density matrix operator, in the presence of decay, is obtained from the Liouville equation as

$$\frac{d}{dt}\rho = -\frac{i}{\hbar}[\mathbf{H}, \rho] + \mathbf{D}\rho, \tag{4}$$

where $\mathbf{D}$ is the relaxation matrix. The density matrix elements obey the conditions $\sum_i \rho_{ii} = 1$ and $\rho_{li} = \rho_{il}^*$. The sources of relaxation in our system are spontaneous emission from the excited state to the lower states with equal decay rates $\Gamma_0/3$

($\Gamma_0 = 10^7$ s^{-1}), transit relaxation of the atoms through the beams from all allowed states with the rate Γ_t ($\approx 10^3$ s^{-1}), the Raman coherence decay with the rate Γ_R ($\approx 10^4$ s^{-1}), and the optical coherence decay rate Γ. In our simple model, we do not explicitly take into account the Doppler effect, but assume that the optical coherence decay rate $\Gamma/2\pi$ would effectively be given by the width ($\approx$0.5 GHz) of the transition in the Doppler-broadened medium. This approximation has already been shown to be valid in the case of EIT in a standard three-level system in ^{4}He* [36,39].

From Eq. (4), the equations of evolution of the density matrix elements $\tilde{\rho}_{mn}(t)$ for the four-level double tripod system interacting with the π- and σ-polarized beams can be written as

$$\frac{d\rho_{g_{\mp}g_{\mp}}(t)}{dt} = \frac{\Gamma_0}{3}\rho_{ee}(t) - \Gamma_t\left[\rho_{g_{\mp}g_{\mp}}(t) - \frac{1}{3}\right]$$
$$+ \frac{i}{2}[X_1^*\tilde{\rho}_{eg_{\mp}}(t) - X_1\tilde{\rho}_{g_{\mp}e}(t)], \qquad (5)$$

$$\frac{d\rho_{g_0g_0}(t)}{dt} = \frac{\Gamma_0}{3}\rho_{ee}(t) - \Gamma_t\left[\rho_{g_0g_0}(t) - \frac{1}{3}\right]$$
$$+ \frac{i}{2}[X_2^*\tilde{\rho}_{eg_0}(t) - X_2\tilde{\rho}_{g_0e}(t)], \qquad (6)$$

$$\frac{d\tilde{\rho}_{eg_{\mp}}(t)}{dt} = -[\Gamma \pm i\Delta_Z]\tilde{\rho}_{eg_{\mp}}(t) + \frac{i}{2}\{X_1[\rho_{g_{\mp}g_{\mp}}(t)$$
$$- \rho_{ee}(t)] + X_2\tilde{\rho}_{g_0g_{\mp}}(t) + X_1\tilde{\rho}_{g_{\pm}g_{\mp}}(t)\}, \qquad (7)$$

$$\frac{d\tilde{\rho}_{eg_0}(t)}{dt} = -\Gamma\tilde{\rho}_{eg_0}(t) + \frac{i}{2}\{X_1[\tilde{\rho}_{g_-g_0}(t) + \tilde{\rho}_{g_+g_0}(t)]$$
$$+ X_2[\rho_{g_0g_0}(t) - \rho_{ee}(t)]\}, \qquad (8)$$

$$\frac{d\tilde{\rho}_{g_{\mp}g_0}(t)}{dt} = -[\Gamma_R \mp i\Delta_Z]\tilde{\rho}_{g_{\mp}g_0}(t)$$
$$+ \frac{i}{2}[X_1^*\tilde{\rho}_{eg_0}(t) - X_2\tilde{\rho}_{g_{\mp}e}(t)], \qquad (9)$$

$$\frac{d\tilde{\rho}_{g_+g_-}(t)}{dt} = -[\Gamma_R + 2i\Delta_Z]\tilde{\rho}_{g_+g_-}(t)$$
$$+ \frac{i}{2}[X_2^*\tilde{\rho}_{eg_-}(t) - X_1\tilde{\rho}_{g_+e}(t)], \qquad (10)$$

where $\tilde{\rho}_{eg_{\mp}} \equiv \rho_{eg_{\mp}}e^{i\omega_C t}$, $\tilde{\rho}_{eg_0} \equiv \rho_{eg_0}e^{i\omega_C t}$, $\tilde{\rho}_{g_{\pm}g_0} \equiv \rho_{g_{\pm}g_0}$, and $\tilde{\rho}_{g_{\pm}g_{\mp}} \equiv \rho_{g_{\pm}g_{\mp}}$.

For a closed atomic system, the population is conserved, i.e.,

$$\rho_{ee} + \rho_{g_0g_0} + \rho_{g_-g_-} + \rho_{g_+g_+} = 1, \qquad (11)$$

and we can eliminate, say, ρ_{ee} from Eqs. (5)–(10). Thus these equations can be written in a matrix form as

$$\dot{\mathbf{R}} = \mathbf{BR} - \mathbf{S}, \qquad (12)$$

where we define

$$\mathbf{R} \equiv (\rho_{g_-g_-}, \rho_{g_0g_0}, \rho_{g_+g_+}, \tilde{\rho}_{g_0g_-}, \tilde{\rho}_{g_0g_+}, \tilde{\rho}_{eg_-}, \tilde{\rho}_{eg_0}, \tilde{\rho}_{eg_+},$$
$$\tilde{\rho}_{g_-g_0}, \tilde{\rho}_{g_+g_0}, \tilde{\rho}_{g_-e}, \tilde{\rho}_{g_0e}, \tilde{\rho}_{g_+e}, \tilde{\rho}_{g_+g_-}, \tilde{\rho}_{g_-g_+})^T$$

and $\mathbf{S}$ is a constant vector.

The equation of motion (12) can be solved for the harmonic terms of δ using the Floquet theorem as has been done in Refs. [40,41]. We expand each term in the equation of motion accordingly as

$$\mathbf{B} = \Omega_P^*\mathbf{B}_{-1}e^{i\delta t} + \mathbf{B}_0 + \Omega_P\mathbf{B}_1e^{-i\delta t}, \qquad (13)$$

$$\mathbf{S} = \Omega_P^*\mathbf{S}_{-1}e^{i\delta t} + \mathbf{S}_0 + \Omega_P\mathbf{S}_1e^{-i\delta t}. \qquad (14)$$

We assume that the probe beam is very weak compared to the coupling beam so that the Floquet harmonic expansion can be truncated at first order [42]:

$$\mathbf{R} = \Omega_P^*\mathbf{R}_{-1}e^{i\delta t} + \mathbf{R}_0 + \Omega_P\mathbf{R}_1e^{-i\delta t}. \qquad (15)$$

Substituting the above equations into Eq. (12) and equating the coefficients of the different harmonics of δ, the steady-state solution of Eq. (12) gives us the recurrence relation for the harmonic terms of $\mathbf{R}$ as

$$\mathbf{R}_0 = \mathbf{B}_0^{-1}\mathbf{S}_0, \qquad (16)$$

$$\mathbf{R}_{\pm} = (\mathbf{B}_0 \pm i\delta)^{-1}(\mathbf{S}_{\pm 1} - \mathbf{B}_{\pm 1})\mathbf{R}_0, \qquad (17)$$

$$\mathbf{S}_q = \mathbf{B}_1\mathbf{R}_{q-1} + [\mathbf{B}_0 + iq\delta]\mathbf{R}_q + \mathbf{B}_{-1}\mathbf{R}_{q+1}, \qquad (18)$$

where $q = 0, \pm 1, \pm 2, \ldots$ and $\mathbf{S}_q$ is nonzero only for $q = 0, \pm 1$.

$$\mathbf{B}_0 = \begin{pmatrix} -\Gamma_a & -\frac{\Gamma_0}{3} & -\frac{\Gamma_0}{3} & 0 & 0 & \Phi_C & 0 & 0 & 0 & 0 & -\Phi_C & 0 & 0 & 0 & 0 \\ -\frac{\Gamma_0}{3} & -\Gamma_a & -\frac{\Gamma_0}{3} & 0 & 0 & 0 & \Psi_C & 0 & 0 & 0 & 0 & -\Psi_C & 0 & 0 & 0 \\ -\frac{\Gamma_0}{3} & -\frac{\Gamma_0}{3} & -\Gamma_a & 0 & 0 & 0 & 0 & \Phi_C & 0 & 0 & 0 & 0 & -\Phi_C & 0 & 0 \\ 0 & 0 & 0 & d & 0 & \Psi_C & 0 & 0 & 0 & 0 & 0 & -\Psi_C & 0 & 0 & 0 \\ 0 & 0 & 0 & 0 & d^* & 0 & 0 & \Psi_C & 0 & 0 & 0 & -\Psi_C & 0 & 0 & 0 \\ 2\Phi_C & \Phi_C & \Phi_C & \Psi_C & 0 & e & 0 & 0 & 0 & 0 & 0 & 0 & 0 & \Phi_C & 0 \\ \Psi_C & 2\Psi_C & \Psi_C & 0 & 0 & 0 & -\Gamma & 0 & \Phi_C & \Phi_C & 0 & 0 & 0 & 0 & 0 \\ \Phi_C & \Phi_C & 2\Phi_C & 0 & \Psi_C & 0 & 0 & e^* & 0 & 0 & 0 & 0 & 0 & 0 & \Phi_C \\ 0 & 0 & 0 & 0 & 0 & 0 & \Phi_C & 0 & d^* & 0 & -\Psi_C & 0 & 0 & 0 & 0 \\ 0 & 0 & 0 & 0 & 0 & 0 & \Phi_C & 0 & 0 & d & 0 & 0 & -\Psi_C & 0 & 0 \\ -2\Phi_C & -\Phi_C & -\Phi_C & 0 & 0 & 0 & 0 & 0 & -\Psi_C & 0 & e^* & 0 & 0 & 0 & -\Phi_C \\ -\Psi_C & -2\Psi_C & -\Psi_C & -\Phi_C & -\Phi_C & 0 & 0 & 0 & 0 & 0 & 0 & -\Gamma & 0 & 0 & 0 \\ -\Phi_C & -\Phi_C & -2\Phi_C & 0 & 0 & 0 & 0 & 0 & 0 & -\Psi_C & 0 & 0 & e & -\Phi_C & 0 \\ 0 & 0 & 0 & 0 & 0 & \Phi_C & 0 & 0 & 0 & 0 & 0 & 0 & -\Phi_C & g & 0 \\ 0 & 0 & 0 & 0 & 0 & 0 & 0 & \Phi_C & 0 & 0 & -\Phi_C & 0 & 0 & 0 & g^* \end{pmatrix}, \qquad (19)$$

$$\mathbf{S}_0 = (-\Gamma_b \quad -\Gamma_b \quad -\Gamma_b \quad 0 \quad 0 \quad \Phi_C \quad \Psi_C \quad \Phi_C \quad 0 \quad 0 \quad -\Phi_C \quad -\Psi_C \quad -\Phi_C \quad 0 \quad 0)^T, \qquad (20)$$

where $\Gamma_a \equiv \Gamma_t + \frac{\Gamma_0}{3}$, $\Gamma_b \equiv \frac{\Gamma_t + \Gamma_0}{3}$ ($\Gamma_a \approx \Gamma_b \approx \Gamma_0/3$ since $\Gamma_t \ll \Gamma_0$), $\Phi_C = \frac{i}{2\sqrt{2}}\Omega_C \cos\theta$, $\Psi_C = \frac{i}{2}\Omega_C \sin\theta$, $d = -(\Gamma_R + i\Delta_Z)$, $e = -(\Gamma + i\Delta_Z)$, $g = -(\Gamma_R + 2i\Delta_Z)$, and the superscript T denotes the transpose of a vector.

$$\mathbf{B}_1 = \frac{i}{2}\begin{pmatrix}
0 & 0 & 0 & 0 & 0 & \Phi_P & 0 & 0 & 0 & 0 & 0 & 0 & 0 & 0 & 0 \\
0 & 0 & 0 & 0 & 0 & 0 & \Psi_P & 0 & 0 & 0 & 0 & 0 & 0 & 0 & 0 \\
0 & 0 & 0 & 0 & 0 & 0 & 0 & \Phi_P & 0 & 0 & 0 & 0 & 0 & 0 & 0 \\
0 & 0 & 0 & 0 & 0 & \Psi_P & 0 & 0 & 0 & 0 & 0 & 0 & 0 & 0 & 0 \\
0 & 0 & 0 & 0 & 0 & 0 & 0 & \Psi_P & 0 & 0 & 0 & 0 & 0 & 0 & 0 \\
0 & 0 & 0 & 0 & 0 & 0 & 0 & 0 & 0 & 0 & 0 & 0 & 0 & 0 & 0 \\
0 & 0 & 0 & 0 & 0 & 0 & 0 & 0 & 0 & 0 & 0 & 0 & 0 & 0 & 0 \\
0 & 0 & 0 & 0 & 0 & 0 & 0 & 0 & 0 & 0 & 0 & 0 & 0 & 0 & 0 \\
0 & 0 & 0 & 0 & 0 & 0 & \Phi_P & 0 & 0 & 0 & 0 & 0 & 0 & 0 & 0 \\
0 & 0 & 0 & 0 & 0 & 0 & \Phi_P & 0 & 0 & 0 & 0 & 0 & 0 & 0 & 0 \\
-2\Phi_P & -\Phi_P & -\Phi_P & 0 & 0 & 0 & 0 & 0 & -\Psi_P & 0 & 0 & 0 & 0 & 0 & -\Phi_P \\
-\Psi_P & -2\Psi_P & -\Psi_P & -\Phi_P & -\Phi_P & 0 & 0 & 0 & 0 & 0 & 0 & 0 & 0 & 0 & 0 \\
-\Phi_P & -\Phi_P & -2\Phi_P & 0 & 0 & 0 & 0 & 0 & 0 & -\Psi_P & 0 & 0 & 0 & -\Phi_P & 0 \\
0 & 0 & 0 & 0 & 0 & \Phi_P & 0 & 0 & 0 & 0 & 0 & 0 & 0 & 0 & 0 \\
0 & 0 & 0 & 0 & 0 & 0 & 0 & \Phi_P & 0 & 0 & 0 & 0 & 0 & 0 & 0
\end{pmatrix}, \quad (21)$$

$$\mathbf{S}_1 = \frac{i}{2}(0 \;\; 0 \;\; 0 \;\; 0 \;\; 0 \;\; 0 \;\; 0 \;\; 0 \;\; 0 \;\; 0 \;\; -\Phi_P \;\; -\Psi_P \;\; -\Phi_P \;\; 0 \;\; 0)^T, \quad (22)$$

$$\mathbf{B}_{-1} = \frac{i}{2}\begin{pmatrix}
0 & 0 & 0 & 0 & 0 & 0 & 0 & 0 & 0 & 0 & -\Phi_P & 0 & 0 & 0 & 0 \\
0 & 0 & 0 & 0 & 0 & 0 & 0 & 0 & 0 & 0 & 0 & -\Psi_P & 0 & 0 & 0 \\
0 & 0 & 0 & 0 & 0 & 0 & 0 & 0 & 0 & 0 & 0 & 0 & -\Phi_P & 0 & 0 \\
0 & 0 & 0 & 0 & 0 & 0 & 0 & 0 & 0 & 0 & 0 & -\Psi_P & 0 & 0 & 0 \\
0 & 0 & 0 & 0 & 0 & 0 & 0 & 0 & 0 & 0 & 0 & -\Psi_P & 0 & 0 & 0 \\
2\Phi_P & \Phi_P & \Phi_P & \Psi_P & 0 & 0 & 0 & 0 & 0 & 0 & 0 & 0 & 0 & \Phi_P & 0 \\
\Psi_P & 2\Psi_P & \Psi_P & 0 & 0 & 0 & 0 & 0 & \Phi_P & \Phi_P & 0 & 0 & 0 & 0 & 0 \\
\Phi_P & \Phi_P & 2\Phi_P & 0 & \Psi_P & 0 & 0 & 0 & 0 & 0 & 0 & 0 & 0 & 0 & \Phi_P \\
0 & 0 & 0 & 0 & 0 & 0 & 0 & 0 & 0 & 0 & -\Psi_P & 0 & 0 & 0 & 0 \\
0 & 0 & 0 & 0 & 0 & 0 & 0 & 0 & 0 & 0 & 0 & 0 & -\Psi_P & 0 & 0 \\
0 & 0 & 0 & 0 & 0 & 0 & 0 & 0 & 0 & 0 & 0 & 0 & 0 & 0 & 0 \\
0 & 0 & 0 & 0 & 0 & 0 & 0 & 0 & 0 & 0 & 0 & 0 & 0 & 0 & 0 \\
0 & 0 & 0 & 0 & 0 & 0 & 0 & 0 & 0 & 0 & 0 & 0 & 0 & 0 & 0 \\
0 & 0 & 0 & 0 & 0 & 0 & 0 & 0 & 0 & 0 & 0 & 0 & -\Phi_P & 0 & 0 \\
0 & 0 & 0 & 0 & 0 & 0 & 0 & 0 & 0 & 0 & -\Phi_P & 0 & 0 & 0 & 0
\end{pmatrix}, \quad (23)$$

$$\mathbf{S}_{-1} = \frac{i}{2}(0 \;\; 0 \;\; 0 \;\; 0 \;\; 0 \;\; \Phi_P \;\; \Psi_P \;\; \Phi_P \;\; 0 \;\; 0 \;\; 0 \;\; 0 \;\; 0 \;\; 0 \;\; 0)^T, \quad (24)$$

where $\Phi_P = \frac{\sin\theta}{\sqrt{2}}$ and $\Psi_P = -\cos\theta$.

The populations of the atomic levels can be obtained from the first three elements of the $\mathbf{R}_0$ vector. The first three elements of the $\mathbf{R}_{\pm 1}$ vector contain information concerning the pulsation of the ground- and excited-level populations at the difference frequency δ between the coupling and the probe beams, and these also provide the information about population redistribution and coherence among Zeeman sublevels in the ground or excited levels due to the simultaneous interaction with the coupling and probe beams [43]. The probe

absorption and dispersion are proportional to the imaginary and real parts of the linear susceptibility and the linear susceptibility of the probe beam can be obtained from three elements of the $\mathbf{R}_{-1}$ vector. The imaginary part of the probe susceptibility $\mathrm{Im}[\chi(\omega_P)]$ is proportional to $\mathrm{Im}(\mu_{eg_-}\Phi_P\rho_{eg_-} + \mu_{eg_0}\Psi_P\rho_{eg_0} + \mu_{eg_+}\Phi_P\rho_{eg_+})$, where $\mu_{eg_0} = -\mu_{eg_0} = \mu_{eg_-} = \mu = 1/\sqrt{3}$. The transmission profiles are generated from $\exp\{-k L \mathrm{Im}[\chi(\omega_P)]\}$, where k is the magnitude of the wave vector of the probe beam and L is the length of the helium cell.
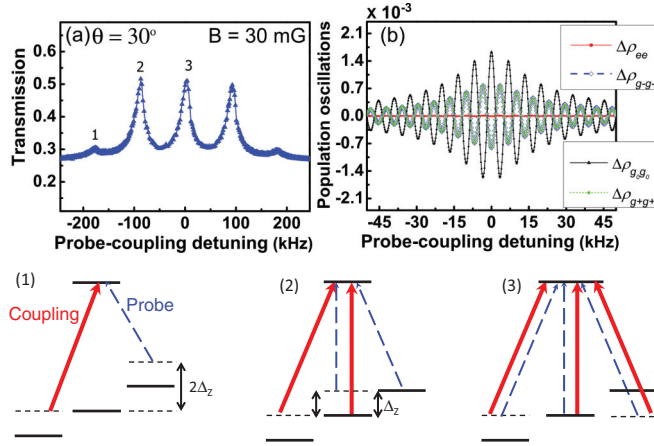
FIG. 2. (Color online) (a) Experimental result of transmission versus probe-coupling detuning obtained for $\theta = 30°$, with magnetic field = 30 mG, and coupling power = 4 mW. The Zeeman shift Δ_Z is 84 kHz. Four peaks can be attributed to EIT as shown in subfigures (1), (2), and (3), where the coupling beam (red continuous line) has a frequency equal to the atomic transition $m = 0 \rightarrow m = 0$ frequency. The small peak labeled 1 on the left is given by the Λ system drawn in subfigure (1) below, the second peak labeled 2 is due to two different Λ systems drawn in subfigure (2). The two peaks on the right are due to symmetrical Λ systems. As shown in subfigure (3), the central resonance happens for coupling and probe beams of the same frequency, which does not correspond to any Raman resonance in the Λ subsystems of the tripod. (b) Amplitudes of the oscillating parts of the populations (at a fixed time) versus δ, with the same Zeeman shift, a coupling Rabi frequency of $\Omega_C/2\pi = 6$ MHz (corresponding to a coupling power of 4 mW), and a Raman coherence decay rate of $\Gamma_R/2\pi = 3$ kHz. $\Delta\rho_{g_+g_+} \equiv 2\text{Re}(\mathbf{R}_{+1})_{31}e^{-i\delta t}$ and $\Delta\rho_{g_-g_-} \equiv 2\text{Re}(\mathbf{R}_{+1})_{11}e^{-i\delta t}$ (blue and green dashed lines) are in phase and oscillate in antiphase with $\Delta\rho_{g_0g_0} \equiv 2\text{Re}(\mathbf{R}_{+1})_{21}e^{-i\delta t}$ (black dotted line), while the excited-state population $\Delta\rho_{ee}$ (red continuous line) does not exhibit any variation.

IV. COMPARISON OF EXPERIMENTAL AND NUMERICAL RESULTS

We record the probe transmission by scanning the probe frequency around the coupling frequency, thus scanning the probe-coupling detuning δ over about 500 kHz around 0. In the absence of the magnetic field ($\Delta_Z = 0$), δ is the two-photon Raman detuning. The experimental result of a probe transmission profile, obtained with a coupling power of 4 mW for an angle $\theta = 30°$ between the probe beam and a 30-mG magnetic field (defining the Z axis), is shown in Fig. 2(a). The coupling beam frequency is chosen equal to the frequency of the atomic transition $m = 0 \rightarrow m = 0$. The small peak labeled 1 on the left is given by the Λ system drawn in subfigure (1): the optical detuning of the pump on the $m = -1 \rightarrow m = 0$ transition is the Zeeman shift $-\Delta_Z \simeq -84$ kHz, which does not introduce a strong asymmetry in the resonance as the Zeeman shift is small compared to the Doppler broadening. Raman resonance is then achieved for the same optical detuning for the probe on the $m = 1 \rightarrow m = 0$ transition, which corresponds to twice the Zeeman shift with respect to the $m = 0 \rightarrow m = 0$ transition frequency. The peak labeled 2 appears when the coupling and probe beam frequency difference is Δ_Z. It is due to two

different Λ systems drawn in subfigure (2): one is at optical resonance (coupling beam on the $m = 0 \rightarrow m = 0$ transition and probe beam on the $m = -1 \rightarrow m = 0$ transition), and the other is optically detuned by $+\Delta_Z$ (coupling beam on the $m = +1 \rightarrow m = 0$ transition and probe beam on the $m = 0 \rightarrow m = 0$ transition). The two symmetrical peaks on the right are due to similar and symmetrical Λ systems. But as shown in subfigure (3), the central resonance appears for coupling and probe beams of the same frequency, which does not correspond to any Raman resonance in the Λ subsystems of the tripod: depending on the Λ subsystem considered, the Raman detuning is $\pm\Delta_Z$ or $\pm2\Delta_Z$.

Indeed, the central peak is a signature of the ground-state CPO, which was also observed in a three-level Λ system (equivalent to two open, interdependent two-level systems) in our previous work [31]. In this case, the two legs of the Λ system are excited by the same pair of coupling and probe fields. The populations in the two ground-state sublevels $|g_\pm\rangle$ are in phase and oscillate in antiphase with the population of the ground level $|g_0\rangle$ as these are driven by intensity modulations which are in antiphase. This is visible in the simulation plotted in Fig. 2(b): the population oscillations of the ground states are plotted with respect to δ (for a given time chosen to make them visible) and show a resonance in amplitude of some kilohertz in width. This induces a transfer of the CPOs between each ground state and the common excited state to CPOs between the two ground states, which gives rise to a sharp central resonance limited by the decay rate of ground-state populations given in our case by the transit time of the atoms through the laser beam. We have checked that no resonance in population oscillations occurs for the values of δ that correspond to the EIT peaks, which confirms that the central and the detuned transmission windows do not come from the same physical phenomenon.

Evidence of the fact that the physical explanation for the central resonance cannot be the same as the side EIT peaks is its sensitivity to the Raman coherence decay rate. We show the numerically calculated transmission profiles for the tripod configuration in Fig. 3 for two different values of the Raman coherence decay rate $\Gamma_R/2\pi$ and for two intermediate θ values of (a) 30° and (b) 60°. It is clearly seen that the EIT resonances, detuned in the presence of the magnetic field
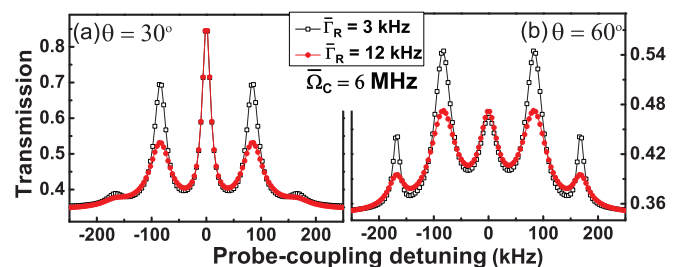

FIG. 3. (Color online) Numerically calculated transmission profiles versus probe-coupling detuning with (a) $\theta = 30°$ and (b) $\theta = 60°$ for $\bar{\Gamma}_R \equiv \Gamma_R/2\pi = 3$ kHz (black squares) and $\Gamma_R/2\pi = 12$ kHz (red dots). Other parameters used are Zeeman splitting $\Delta_Z/2\pi = 84$ kHz (corresponding to a magnetic field, $B = 30$ mG) and coupling Rabi frequency $\bar{\Omega}_C \equiv \Omega_C/2\pi = 6$ MHz (corresponding to a coupling power of 4 mW).
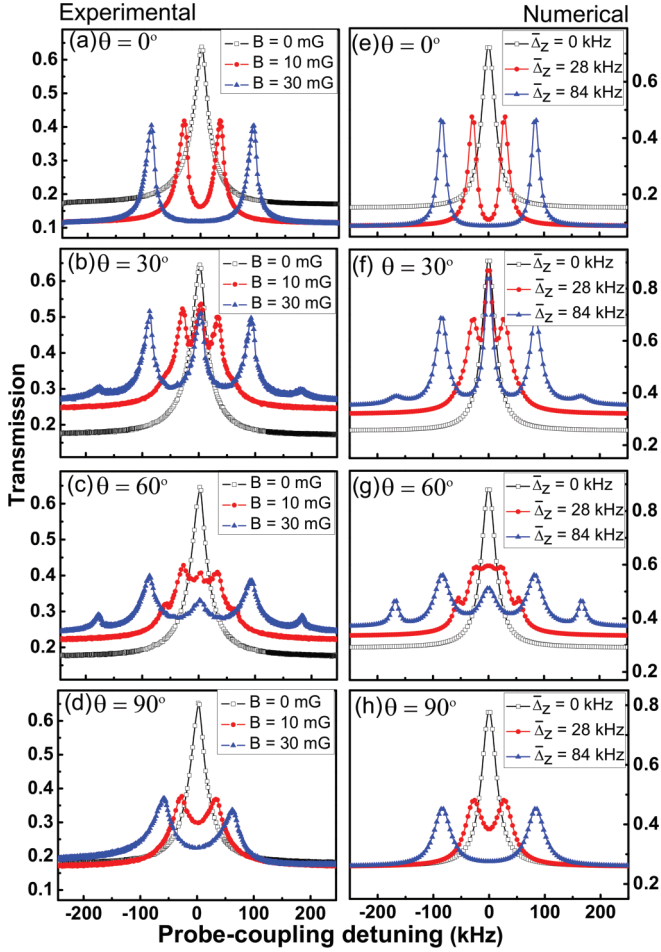
FIG. 4. (Color online) Transmission profiles versus probe-coupling detuning for the double tripod system. (a)–(d) Experimentally measured with magnetic fields at 0 mG (black squares), 10 mG (red dots), and 30 mG (blue triangles), at coupling power = 4 mW. (e)–(h) Numerically calculated with Zeeman splitting $\bar{\Delta}_Z \equiv \Delta_Z/2\pi = 0$ kHz (black squares), $\Delta_Z/2\pi = 28$ kHz (red dots), and $\Delta_Z/2\pi = 84$ kHz (blue triangles), at coupling Rabi frequency $\Omega_C/2\pi = 6$ MHz with the Raman coherence decay rate $\Gamma_R/2\pi = 3$ kHz.
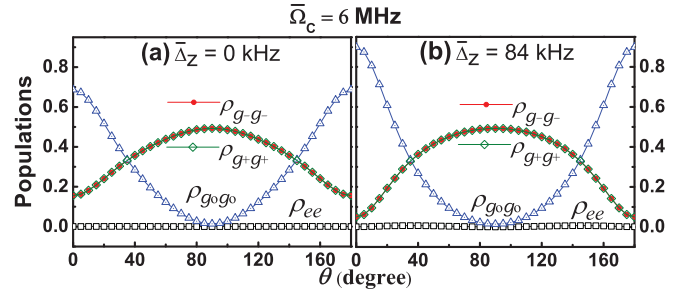

FIG. 5. (Color online) Variation of populations, ρ_{ee} (black squares), $\rho_{g_-g_-}$ (red dots), $\rho_{g_0g_0}$ (blue triangles), and $\rho_{g_+g_+}$ (green rhombuses), with rotation angle θ for (a) $\bar{\Delta}_Z \equiv \Delta_Z/2\pi = 0$ ($B = 0$) and (b) $\Delta_Z/2\pi = 84$ kHz ($B = 30$ mG), with coupling Rabi frequency $\bar{\Omega}_C \equiv \Omega_C/2\pi = 6$ MHz (corresponding to a coupling power of 4 mW) and Raman coherence decay rate $\Gamma_R/2\pi = 3$ kHz.

($\Delta_Z/2\pi = 84$ kHz or $B = 30$ mG), are extremely sensitive to the Raman coherence, but the central peak is unaffected by a change in Γ_R. This proves that the Raman coherence is not involved in this central resonance, which, as explained above, is the consequence of a transfer of CPOs between each ground state and the excited state to CPOs between the state $|g_0\rangle$ and the states $|g_\pm\rangle$.

The left panels in Fig. 4 show the transmission profiles recorded in our experiment for a coupling power of 4 mW; a magnetic field of 0, 10, and 30 mG; and four different θ values. The right panels in Fig. 4 show the corresponding numerical simulations obtained with the Floquet expansion described in Sec. III. The configurations (a) [or (e)] and (d) [or (h)] are for $\theta = 0$ and $90°$, respectively, which correspond to the two configurations considered in Ref. [25]. In the first case ($\theta = 0°$) with π-polarized probe and $\sigma_\pm$-polarized coupling beams, the EIT resonances split by the magnetic field interfere destructively, while in the second case ($\theta = 90°$)

with π-polarized coupling and $\sigma_\pm$-polarized probe beams, the EIT resonances add incoherently. This can be understood from the fact that the dark states induced by the σ-polarized coupling beams are roughly $|g_0\rangle$ for both but with different phases, which cannot be satisfied simultaneously by the same π-polarized probe beam. In the second case, we need to consider two Λ systems that give two different dark states $|g_\pm\rangle$, which do not interfere.

It is visible that there is a change in the background level (transmission level in the wings) with and without the magnetic field for $\theta = 0°$ [Figs. 4(a) and 4(e)], unlike for $\theta = 90°$ [Figs. 4(d) and 4(h)]. To understand this effect, we plot the average populations, ρ_{ee}, $\rho_{g_0g_0}$, and $\rho_{g_\pm g_\pm}$ (given by the first three elements of the $\mathbf{R}_0$ vector), versus the rotation angle θ for (a) zero magnetic field and (b) a moderately high (30 mG) magnetic field. The result is shown in Fig. 5. When $\theta = 0°$, in the absence of the magnetic field, the optical pumping of the population into the probe ground level is not perfect ($\rho_{g_0g_0} < 0.7$) [Fig. 5(a)], and in the presence of the 30-mG magnetic field, it improves to $\rho_{g_0g_0} > 0.9$ [Fig. 5(b)], resulting in more probe absorption (or less probe transmission) in the wings. For intermediate cases in which the excitations on each of the three optical transitions are mixed, the background level variations can be explained by adding the absorption of the probe on each transition.

For the intermediate cases of $\theta = 30°$ [Figs. 4(b) and 4(f)] and $\theta = 60°$ [Figs. 4(c) and 4(g)], as has already been explained using Fig. 2, the four symmetrically detuned transmission peaks at $\pm\Delta_Z$ and $\pm2\Delta_Z$ are due to EIT resonances. The central peak is a signature of CPO. For these intermediate values of θ, both coupling and probe excite the three transitions, which leads to intensity beats that give a transmission window when the frequency of the beats is less than the population decay rate. For the usual CPO in a two-level system, the relevant population decay rate is the decay rate of the upper level, which is much larger (about 1.6 MHz) than the Raman coherence decay rate. In our case, as coupling and probe polarizations are orthogonal, the beats on the σ transitions are in opposite phase with respect to the beats on the π transition. This explains a transfer of the oscillations to population oscillations between $|g_0\rangle$ and $|g_\pm\rangle$, which is then limited by the ground-state decay rate given by the transit rate of atoms through the beam. The amplitude of the oscillation

is maximum for $\theta = 45°$, when both coupling and probe laser are equally shared on the σ and π transitions. We have checked that these oscillations disappear for angles of $0°$ and $90°$, when coupling and probe beams do not excite the same transitions so that no CPO phenomenon can occur.

Our experimental results in all the cases match very well with the numerical simulations done using the Floquet method. It is seen that the height of the central CPO resonance and the EIT peaks can be manipulated by rotating the coupling-probe polarizations.

V. CONCLUSIONS

In conclusion, we have studied a four-level double tripod system using metastable helium gas at room temperature, in which transmission resonances due to both EIT and CPO are established. In this system, we can manipulate EIT and CPO resonances by rotating the orthogonally polarized coupling-probe beams with respect to the quantization axis, defined by a magnetic field. The heights of the EIT and CPO resonance peaks are dependent on the polarization direction. Also, the appearance and disappearance of the central CPO resonance can be controlled by rotating the coupling-probe polarizations. This system can, in principle, be useful as a polarization-dependent switch [44] in the presence of a magnetic field.

Our experimental results match fairly well with our numerical simulations using the Floquet method. Our work may lead to further studies related to elliptically polarized excitations in three-level Λ systems [45,46] and to the explanation of the central resonance dip [47] observed with nonorthogonally polarized coupling-probe beams.

[1] S. E. Harris, J. E. Field, and A. Imamoglu, Phys. Rev. Lett. **64**, 1107 (1990).

[2] K.-J. Boller, A. Imamoglu, and S. E. Harris, Phys. Rev. Lett. **66**, 2593 (1991).

[3] S. E. Harris, Phys. Today **50**, 36 (1997).

[4] M. D. Lukin, Rev. Mod. Phys. **75**, 457 (2003).

[5] E. E. Mikhailov, V. A. Sautenkov, I. Novikova, and G. R. Welch, Phys. Rev. A **69**, 063808 (2004).

[6] M. D. Stenner, D. J. Gauthier, and M. A. Neifeld, Phys. Rev. Lett. **94**, 053902 (2005).

[7] M. Fleischhauer, A. Imamoglu, and J. Marangos, Rev. Mod. Phys. **77**, 633 (2005).

[8] D. F. Phillips, A. Fleischhauer, A. Mair, R. L. Walsworth, and M. D. Lukin, Phys. Rev. Lett. **86**, 783 (2001).

[9] M. Lobino, C. Kupchak, E. Figueroa, and A. I. Lvovsky, Phys. Rev. Lett. **102**, 203601 (2009).

[10] A. I. Lvovsky, B. C. Sanders, and W. Tittel, Nat Photonics **3**, 706 (2009).

[11] B. Julsgaard, J. Sherson, J. I. Cirac, J. Fiuasek, and E. S. Polzik, Nature (London) **432**, 482 (2004).

[12] D. Budker, W. Gawlik, D. F. Kimball, S. M. Rochester, V. V. Yashchuk, and A. Weis, Rev. Mod. Phys. **74**, 1153 (2002).

[13] V. I. Yudin, A. V. Taichenachev, Y. O. Dudin, V. L. Velichansky, A. S. Zibrov, and S. A. Zibrov, Phys. Rev. A **82**, 033807 (2010).

[14] S. E. Harris and L. V. Hau, Phys. Rev. Lett. **82**, 4611 (1999).

[15] N. Sangouard, C. Simon, H. de Riedmatten, and N. Gisin, Rev. Mod. Phys. **83**, 33 (2011).

[16] H. J. Kimble, Nature (London) **453**, 1023 (2008).

[17] J. Martin, B. W. Shore, and K. Bergmann, Phys. Rev. A **54**, 1556 (1996).

[18] F. Vewinger, M. Heinz, R. Garcia Fernandez, N. V. Vitanov, and K. Bergmann, Phys. Rev. Lett. **91**, 213001 (2003).

[19] R. G. Unanyan, M. E. Pietrzyk, B. W. Shore, and K. Bergmann, Phys. Rev. A **70**, 053404 (2004).

[20] M. D. Lukin, S. F. Yelin, M. Fleischhauer, and M. O. Scully, Phys. Rev. A **60**, 3225 (1999).

[21] S. F. Yelin, V. A. Sautenkov, M. M. Kash, G. R. Welch, and M. D. Lukin, Phys. Rev. A **68**, 063801 (2003).

[22] F. A. Hashmi and M. A. Bouchene, Phys. Rev. A **77**, 051803(R) (2008).

[23] M. A. Antòn and F. Carreño, J. Opt. **12**, 104006 (2010).

[24] D. Petrosyan and Y. P. Malakyan, Phys. Rev. A **70**, 023822 (2004).

[25] S. Kumar, T. Lauprêtre, R. Ghosh, F. Bretenaker, and F. Goldfarb, Phys. Rev. A **84**, 023811 (2011).

[26] S. E. Schwartz and T. Y. Tan, Appl. Phys. Lett. **10**, 4 (1967).

[27] R. W. Boyd, M. G. Raymer, P. Narum, and D. J. Harter, Phys. Rev. A **24**, 411 (1981).

[28] F. Ohman and K. Yvind, IEEE Photonics Technol. Lett. **19**, 1145 (2007).

[29] E. Shumakher, S. O. Duill, and G. Eisenstein, J. Lightwave Technol. **27**, 4063 (2009).

[30] P. Berger, J. Bourderionnet, F. Bretenaker, D. Dolfi, and M. Alouini, Opt. Express **19**, 21180 (2011).

[31] T. Lauprêtre, S. Kumar, P. Berger, R. Faoro, R. Ghosh, F. Bretenaker, and F. Goldfarb, Phys. Rev. A **85**, 051805(R) (2012).

[32] P. R. Berman, D. G. Steel, G. Khitrova, and J. Liu, Phys. Rev. A **38**, 252 (1988).

[33] C. Goren, A. D. Wilson-Gordon, M. Rosenbluh, and H. Friedmann, Phys. Rev. A **70**, 043814 (2004).

[34] A. Eilam, I. Azuri, A. V. Sharypov, A. D. Wilson-Gordon, and H. Friedmann, Opt. Lett. **35**, 772 (2010).

[35] A. V. Sharypov and A. D. Wilson-Gordon, Phys. Rev. A **84**, 033845 (2011).

[36] J. Ghosh, R. Ghosh, F. Goldfarb, J.-L. Le Gouët, and F. Bretenaker, Phys. Rev. A **80**, 023817 (2009).

[37] G.V. Shlyapnikov, J. T. M. Walraven, U. M. Rahmanov, and M. W. Reynolds, Phys. Rev. Lett. **73**, 3247 (1994).

[38] N. Gavra, M. Rosenbluh, T. Zigdon, A. D. Wilson-Gordon, and H. Friedmann, Opt. Commun. **280**, 374 (2007).

[39] F. Goldfarb, J. Ghosh, M. David, J. Ruggiero, T. Chanelière, J.-L. Le Gouët, H. Gilles, R. Ghosh, and F. Bretenaker, Europhys. Lett. **82**, 54002 (2008).

[40] V. Wong, R. W. Boyd, C. R. Stroud, Jr., R. S. Bennink, D. L. Aronstein, and Q-H. Park, Phys. Rev. A **65**, 013810 (2001).

[41] R. W. Boyd, *Nonlinear Optics* (Academic Press, San Diego, 2003).

[42] We have checked that the higher-order terms in the expansion do not make any significant contribution to our results.

[43] A. Lezama, S. Barreiro, A. Lipsich, and A.M. Akulshin, Phys. Rev. A **61**, 013801 (1999).

[44] U. Khadka, Y. Zhang, and M. Xiao, Phys. Rev. A **81**, 023830 (2010).

[45] S. A. Zibrov, V. L. Velichansky, A. S. Zibrov, A. V. Taichenachev, and V. I. Yudin, Opt. Lett. **31**, 2060 (2006).

[46] A.V. Taichenachev, V. I. Yudin, V. L. Velichansky, A. S. Zibrov, and S. A. Zibrov, Phy. Rev. A **73**, 013812 (2006).

[47] A. D. Wilson-Gordon and H. Friedmann, Opt. Lett. **14**, 390 (1989).